Effects of particle properties on segregation-band drift in particle-laden rimming flow

E. Guyez[a] and P. J. Thomas[b]
Fluid Dynamics Research Centre, School of Engineering, University of Warwick, Coventry CV4 7AL, United Kingdom

(Received 24 July 2008; accepted 10 January 2009; published online 17 March 2009)

We experimentally study rimming flow of a particle-laden fluid. We begin to investigate the details of the spatiotemporal segregation-band dynamics that were first documented by us elsewhere [E. Guyez and P. J. Thomas, Phys. Rev. Lett. **100**, 074501 (2008)]. There exist eight relevant nondimensional parameters that must be expected to affect the drift dynamics of segregation bands in particle-laden rimming flow. Here we summarize results from experiments investigating the effects of three of these parameters that involve the particle size and the particle density. It is shown that two of the parameters are crucial to the initiation of the band drift and that bands become stationary whenever either one of the two parameters adopts values below an associated critical threshold. Based on the physical relevance of the two parameters it is concluded that the initiation of band drift is strongly affected by a competition between capillary forces and gravitational forces. The third nondimensional parameter studied here characterizes the bulk particle concentration and it is found that it controls the band-drift speed in the parameter regime where band drift exists.
 [DOI: 10.1063/1.3081046]

I. INTRODUCTION

In Refs. 1 and 2 we reported a new segregation phenomenon in a simple, generic flow configuration commonly referred to as rimming flow. Rimming flow is the flow established inside a partially fluid-filled cylinder when it rotates around a horizontal axis of rotation. In Refs. 1 and 2 we investigated rimming flow for the case when the liquid carries small particles with densities higher or lower than that of the fluid. It was found that the particles can segregate to form a series of successive granule-rich azimuthal bands separated from one another by fluid regions with lower particle concentrations or regions entirely free of granules as illustrated in Fig. 1.

Banding patterns appearing similar to those discussed by Boote and Thomas[1] were also observed in suspensions of heavy particles within a fully filled horizontal rotating cylinder,[3,4] as well as in suspensions containing neutrally buoyant particles in a horizontal Taylor–Couette system[5–7] and in rimming flows.[8] However, it is not yet clear in how far the patterns in the different systems, and under the different experimental conditions, do indeed all represent the same physical phenomenon. For the particular case of rimming flow where the liquid carries neutrally buoyant particles Jin and Acrivos[9,10] proposed a model for the band formation that is based on an axially varying viscosity. An associated linear stability analysis for dilute suspensions showed that such a particle distribution is unstable to axial perturbations. The calculated and measured spacings between the bands were found to be in good agreement.[8,10] Nevertheless, this model may not be appropriate for rimming flow where the particles are not neutrally buoyant. For instance, the model[9,10] cannot explain the triplet fine structure observed by Thomas *et al.*[2] for rimming flow with particles less dense than the ambient liquid.

Recently the problem of segregation banding in particle-laden rimming flow became further involved since Guyez and Thomas[11] reported that the banding patterns in suspensions of heavy particles can display a very complex and often highly symmetric spatiotemporal behavior that emerges on time scales of days or weeks as the granule bands drift very slowly along the direction of the cylinder axis. They identified a number of different characteristic drift modes which are not known to exist for rimming flows of neutrally buoyant particles. For instance, Guyez and Thomas[11] observed that depending on the experimental conditions, the bands can either drift from the end walls of the cylinder toward its center or, alternatively, from positions along the cylinder axis toward the end walls. Sometimes the bands oscillate irregularly in space and time and sometimes they remain entirely stationary. The purpose of the present experiments was to begin to explore in detail in which regions of the parameter space the system adopts the different characteristic drift modes.

II. EXPERIMENTAL METHODS AND PARAMETERS

A. Experimental setup

The experiments were performed with the same apparatus used for our previous studies[1,2,11] The facility is shown in Fig. 1 and consists of a transparent circular cylinder that is rotated around a horizontal axis of rotation by means of a variable-speed motor and a pulley-and-belt drive. The acrylic cylinder (Blanson Ltd., Leicester) has a length $l_0=27$ cm and a radius of $r_0=5$ cm. The cylinder can be leveled by

[a]Electronic mail: estelle.guyez@cea.fr.
[b]Electronic mail: pjt1@eng.warwick.ac.uk.

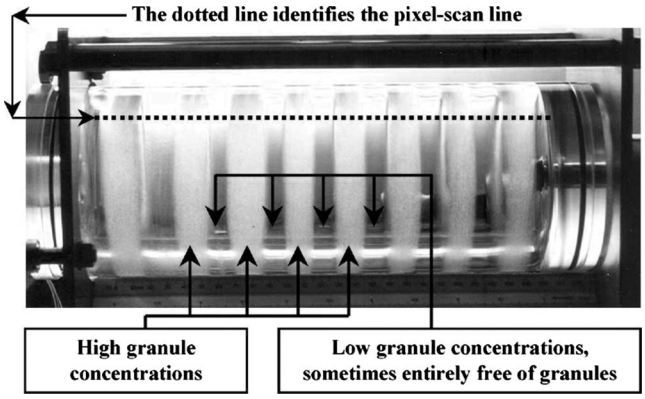

FIG. 1. Segregation banding pattern in horizontal circular cylinder viewed head-on.

means of three leveling screws protruding from the bottom side of the support plate on which the facility and its auxiliary equipment is mounted. High-precision horizontal leveling is essential to ensure that the band drift is not biased due to cylinder misalignment. We determined that the band-drift dynamics become affected when the inclination angle of the cylinder, with respect to the horizontal, exceeds a few minutes of a degree.

The experiments were conducted in a temperature-controlled room at a temperature of 21 ± 0.5 °C. The working fluid is silicone oil (Ambersil, F111/500). We measured the volume and weight of a sample of the liquid and determined a density of $\rho = 1.108$ g cm^{-3} varying less than 0.5% over a temperature interval of 21 ± 1 °C. The viscosity of the silicone oil was measured by means of a Brookfield digital viscometer (Model DV-E). A viscosity of $\mu = 480$ mPa s, with 3% variations over the same temperature interval, was found. A ring tensiometer yielded a value of $\sigma = 21.2$ mN m^{-1} for the surface tension at the reference temperature. The filling fraction of the cylinder is, for all experiments, equal to $F = V_F/V = 0.14$, where V_F represents the volume of the fluid and V is the volume of the cylinder.

Different types of particles were used depending on the particular goal of each experiment. Most experiments were conducted using spherical glass particles of density $\rho_g = 2.5$ g cm^{-3} (Omya). The mean diameters of the glass particles were in the range $0.2 \text{ mm} \leq d_g \leq 1.1$ mm. The maximum deviation from the mean, as stated by the manufacturer, is ± 100 μm for the larger type of particles and ± 50 μm for the smaller ones. We also performed experiments with polyamide, sugar and metal particles of similar mean diameter and associated particle densities which are 1.13, 1.64, and 7.1 g cm^{-3}, respectively.

In order to clearly establish the nature of the band-drift dynamics it is required that depending on the experimental conditions, experiments have to run for at least a day but often for several days or even weeks (see also Guyez and Thomas[11]). To monitor the experiments we used a programmable digital camera (Nikon D100) with a pixel resolution of 2500×3500. Photographs were taken at intervals, Δt of 10, 20, or 60 s, depending on the anticipated band-drift velocity in any particular experiment. The photographs were transferred *in situ* to a PC for storage and data processing. For the data processing of each photograph we extracted a horizontal pixel line at a position corresponding approximately to that indicated in Fig. 1 by the dotted line. Each pixel line was processed such that the location of the bands with high particle concentrations is represented in black whereas granule-free regions or regions with low particle concentrations appear in white. The pixel lines extracted from the successive photographs of an experiment were then stacked into a single image to compose a spatiotemporal plot. This type of plot reveals the drift of the granule bands and thereby illustrates the overall system dynamics.

B. Governing nondimensional parameters

There exist eight nondimensional parameters that can affect the flow dynamics. Jin and Acrivos[9,10] derived seven of these parameters, for the case of neutrally buoyant particles, and we have added one further parameter to account for density differences between the particles and the ambient fluid. The first parameter is the filling fraction, $F = V_F/V$, of the cylinder that was already defined in Sec. II A. The next parameter is the Reynolds number, $\text{Re} = \rho\omega h^2/\mu$, where ω is the rotational velocity of the cylinder and h is the mean film thickness of the liquid film on the inner cylinder wall when the cylinder rotates. The parameter $\alpha = \sqrt{\mu\omega/\rho g r_0}$, where g is the gravitational acceleration, characterizes the ratio of viscous and gravitational forces. A capillary number, $\gamma = \sigma/\rho g r_0^2$, describes the ratio of surface tension and gravity. The parameter $\delta = h_m/d_g$ characterizes the ratio between the minimum film thickness, h_m, and the mean diameter, d_g, of the granules (according to Joseph *et al.*,[12] $h_m = 0.596\alpha r_0$). The bulk proportion of granules within the fluid is referred to by $\phi = V_g/V_F$, where V_g is the volume occupied by the granules and V_F is the fluid volume. The aspect ratio of the cylinder is $\chi = l_0/r_0$. To account for the density difference between liquid and particles we define a Stokes number, $\text{St} = (\rho_g - \rho) g d_g^2/18\omega\mu r_0$. This Stokes number is the only new nondimensional parameter introduced here. It was not previously required in Jin and Acrivos[9,10] since they used neutrally buoyant particles only. The Stokes number represents the ratio between the settling velocity of the particles and the rotational velocity of the cylinder and also characterizes the ratio of the drag force and the buoyancy forces acting on the particles. Here we begin to investigate details of the effects of St, δ and St=0.049, and ϕ on the spatiotemporal drift dynamics of the segregation bands.

The large number of nondimensional parameters involved in the problem is indicative of the complexity of the band-drift dynamics described in Guyez and Thomas.[11] The definitions of several of the nondimensional parameters share some of the same quantities among them. For instance, the particle size, d_g, appears both in the definition of the Stokes number and in the definition of the parameter δ. Hence, altering the particle size results in simultaneous changes of both these nondimensional numbers. Similar problems arise for other particle and fluid characteristics in connection with the remaining nondimensional parameters. This implies that

TABLE I. Dimensional parameters for the reference experiment, RE.

r_0 (mm)	l_0 (mm)	ω (rad s^{-1})	μ (mpa s)	ρ (g mm^{-3})	V (ml)	m_g (g)	ρ_g (g cm^{-3})	d_{min} (μm)	d_{max} (μm)
50	270	0.52	480	1.108	300	60	2.5	250	425

establishing the individual effects of each of the nondimensional parameters is not a straightforward process.

III. RESULTS AND DISCUSSION

A. Reference experiment

Experiments were carried out for a wide range of the governing independent experimental parameters. We select one set of experimental conditions (see Tables I and II) as a reference experiment and refer to this case as RE. Phase space was explored by conducting experiments for which each time only one or two of the independent physical parameters that are investigated differed from those of RE. Note that for all experiments the ratio F/α exceeds the critical value of 1.6 identified in the context of Jin and Acrivos.[9,10] (Note that in Ref. 11, we erroneously quoted a critical threshold of $\beta=F/\alpha=0.7$ rather than the correct value of 1.6.)

The spatiotemporal diagram illustrating the band-drift dynamics of RE is shown in Fig. 2. The position, L, along the cylinder axis is shown on the abscissa where $L=0$ corresponds to the left and $L=27$ cm to the right end wall of the cylinder. The ordinate on the left-hand side of the plot displays time, t, in terms of the number of cylinder revolutions, t/T, where T is the time required for one complete revolution of the cylinder. Additionally the ordinate on the right-hand side of the plot displays time in units of days in order to provide a better feel for the time scales involved in the experiments. Inspection of Fig. 2 reveals the complex and highly symmetric drift dynamics of the experiment. The band drift is directed from positions along the cylinder axis toward the left and right end walls. The bands accelerate as they approach the end walls. Further details of RE were discussed by Guyez and Thomas.[11]

B. Effect of the granule concentration on the band-drift dynamics

For the experiments discussed in this section the granule concentration is the only quantity differing from the conditions of RE. The experiments of this section will be referred to as series GC. As summarized in Table III the mass of the particles added is increased in ten successive steps (GC1–GC10) from 20 mg to 240 g such that the bulk concentration is $0.0027\% \leq \phi \leq 32\%$.

TABLE II. Nondimensional parameters for the reference experiment, RE.

Re	α	F	γ	χ	ϕ	δ	St
0.016	0.022	14%	0.0008	5.2	8%	1.88	0.007

Well-defined bands were first identified for GC2 with $\phi > 0.027\%$; corresponding to about 4000 particles. This threshold is below that in Boote and Thomas.[1] At very low particle concentrations it required 300 min before bands could be identified. In their original experiments, Boote and Thomas[1] did not observe the system over sufficiently long intervals to enable them to identify bands at lowest concentrations. The time scale for band formation decreases with increasing particle concentration. At $\phi=0.27\%$ we identified bands after 60 min while for the higher concentrations bands typically form in less than 1 min. In GC1, for the lowest particle concentration tested, most particles were still randomly distributed throughout the liquid film on the inner cylinder surface after 1 day of continuous cylinder rotation. Nevertheless, there was a somewhat higher concentration of granules in the vicinity of the end walls.

Figures 3–5 show the spatiotemporal evolution of three typical cases of the series GC1–GC10. The data shown are for GC3, GC4, and GC8 with $\phi=0.27\%$, $\phi=2.7\%$, and $\phi=16\%$, respectively, of particles added. Together with Fig. 2 for RE these plots provide a representative overview of the dynamics displayed by the whole series. One observes that changing the amount of particles added does not affect the direction of the band drift. In all the cases the bands drift toward the two end walls of the cylinder.

Figures 2–5 also reveal that band-drift velocities are low near the cylinder center and that bands always accelerate as they approach the end walls. The plots for the lowest and highest particle concentrations, in Figs. 3 and 5, suggest the existence of a characteristic length scale where wall effects affect the drift dynamics. In Fig. 3 the leftmost and rightmost bands appear to be attracted by the walls while the five central bands remain stationary. For higher particle concentra-

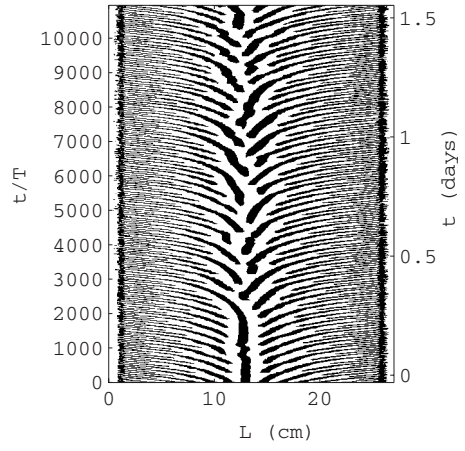

FIG. 2. Spatiotemporal evolution of the position of the granule bands in the reference experiment, RE, with $\phi=8\%$.

TABLE III. Mass of particles added and modified parameters for experiments GC1–GC10.

	Expt.									
	GC1	GC2	GC3	GC4	GC5	GC6	GC7	GC8	GC9	GC10
m (g)	0.02	0.2	2	20	40	80	100	120	180	240
ϕ (%)	0.0027	0.027	0.27	2.7	5.3	10.7	13.3	16	24	32

tions, as in the experiment GC8 of Fig. 5, there exist two clear boundaries, at $L \approx 9$ cm and at $L \approx 18$ cm, separating the central cylinder section from the left and right wall-near zones. Note that no new bands are formed within in the edge zones. We believe that the existence of the well-defined wall-near zones, and also the acceleration of the bands as they approach the end walls, clearly suggests that the flow induced in the vicinity of the end walls plays a key role in governing, and possibly sustaining, the band drift. For the intermediate particle concentrations, i.e., in Figs. 2 and 4, the boundaries between the central zone and the wall-near regions are less well defined. Nevertheless, similar to the experiments with higher particle concentrations no new bands form within a distance of approximately 3–4 cm from the end walls.

For GC2 and GC3 (Fig. 3), the two experiments with the smallest particle concentrations where proper bands develop, the disappearance of bands near the walls is not followed by the successive formation of new bands as is the case for the higher particle concentrations (Figs. 2, 4, and 5). For the experiments with low particle concentrations this implies that the particles contained within the bands reaching the end walls are deposited in the vicinity of the wall and then remain there; there exists no particle recirculation. A recirculation is required by continuity, for indefinitely running experiments with higher particle concentrations where new bands are continuously generated, if the band drift is associated with a net particle transport.[11]

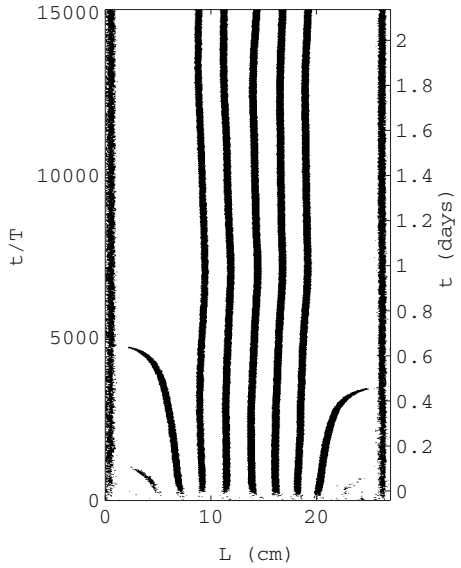

FIG. 3. Spatiotemporal evolution of the position of the granule bands in GC3 with ϕ=0.27%.

Figures 3–5 reveal further fundamental qualitative differences between the drift dynamics for low- and high-concentration experiments. In Fig. 3 the five central bands, located between approximately L=9 cm and L=18 cm, do not move at all. This means that the particle concentration is sufficiently low to enable bands to arrange in such a way that neighboring bands are not located within their mutual region of influence. For intermediate particle concentrations (Figs. 2 and 4) the bands are sufficiently close together such that they synchronize their motion. All bands drift in phase, to the left in the left half of the cylinder and to the right in the right half of the cylinder. The appearance of a new band does not affect the drift direction of any existing band. However, for the higher particle concentrations, as for GC8 (Fig. 5) or GC9 and GC10, the bands are sufficiently close together that the emergence of a new band can induce a change in the drift direction of a neighboring band. This is illustrated in Fig. 6 which constitutes an enlarged representation of the region 7 cm$\leq L \leq$20 cm and 500$\leq t/T \leq$2500 of Fig. 5. Consider the two bands that start above the two letters A and B in Fig. 6. Band A is generated in the left half of the cylinder ($L \approx 10$ cm) but initially drifts toward the right and into the right half of the cylinder ($L > 13.5$ cm). At $t/T \approx 2000$ the drift direction of band A changes abruptly and the band now begins to drift leftward. This change of the drift direction occurs precisely at that instance as band B has formed to the left of A and begins to drift to the left. Inspection of Fig. 5 reveals that there are several other similar events present within the diagram.

Figure 7 displays the drift velocity, U, of the bands as a function of their location, L, and the particle concentration,

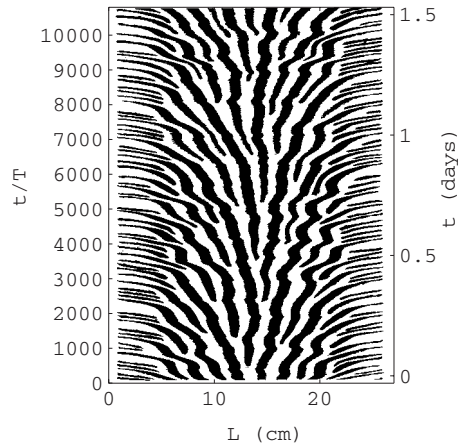

FIG. 4. Spatiotemporal evolution of the position of the granule bands in GC4 with ϕ=2.7%.

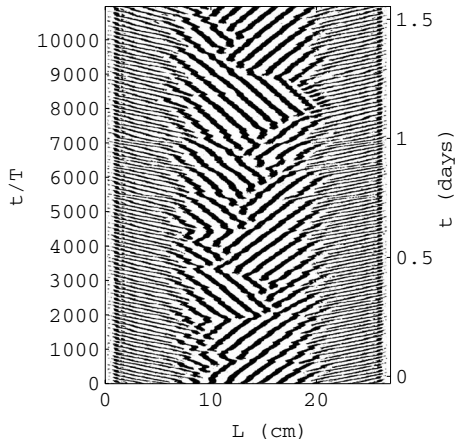

FIG. 5. Spatiotemporal evolution of the position of the granule bands in GC8 with $\phi=16\%$.

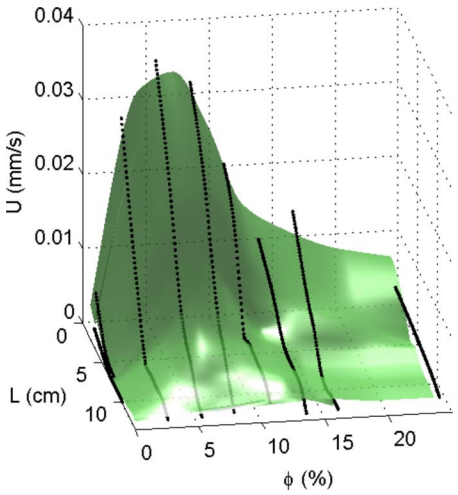

FIG. 7. (Color online) The drift velocity, U, of bands in RE and GC3–GC10 as a function of position, L, and particle concentration, ϕ. The data are for the left half of the cylinder ($0<L<13.5$ cm). The black, solid lines represent the experimental data and the interstitial regions have been interpolated.

ϕ. Since all experiments display a high symmetry for the dynamics in the left and right half of the cylinder only the data for the left half ($L\leq l_0/2=13.5$ cm) are displayed. The graph quantitatively illustrates how the bands accelerate as they approach the end wall, i.e., for $L\rightarrow 0$. An acceleration is observed for all particle concentrations, ϕ. However, maximum drift velocities are adopted for experiments with intermediate particle concentrations around $5.3\%\leq\phi\leq 8\%$ (note that 8% is the concentration of RE).

The existence of a maximum drift velocity in Fig. 7 is probably the consequence of two competing effects. For particle concentrations $\phi\leq 5.3\%$ (GC3, GC4, GC5) increasing concentrations lead to stronger band interactions resulting in higher drift velocities. However, increasing particle concentrations also result in a higher effective viscosity of the particle-laden liquid. It appears plausible that above $\phi\approx 8\%$ (Re, GC6–GC10) the decelerating viscosity increase outweighs the accelerating band-interaction effects resulting in an overall net reduction of the drift velocities. In this context we briefly comment on the degree of the axial particle segregation. We observed that for GC1–GC5 segregation is complete, in the sense that the space between the bands is completely devoid of particles, while the segregation is incomplete for RE and GC6–GC10. Hence, the band-drift velocity increases with the particle concentration while segregation is complete. However, it decreases with increasing particle concentration when segregation is incomplete.

Figure 8 displays the number of bands, N_b (circles and left ordinate), and the band width, W (squares and right ordinate), as a function of the particle concentration, ϕ. The bandwidth was measured at the highest point of the cylinder where the bands are narrowest. Both N_b and W represent values averaged over the duration of the experiment and the error bars displayed in Fig. 8 indicate the minimum and maximum values adopted by the two parameters.

Figure 8 reveals that increasing particle concentrations lead to an increase in the total number of bands. Effects of the particle concentration on the number of bands were not observed by Boote and Thomas[1] and Thomas *et al.*[2] since the particle concentrations in their experiments were only varied over a substantially narrower interval than in the present study. Here the values for the particle concentration extend over four orders of magnitude, in terms of ϕ, compared to increases of less than one order of magnitude in Refs. 1 and

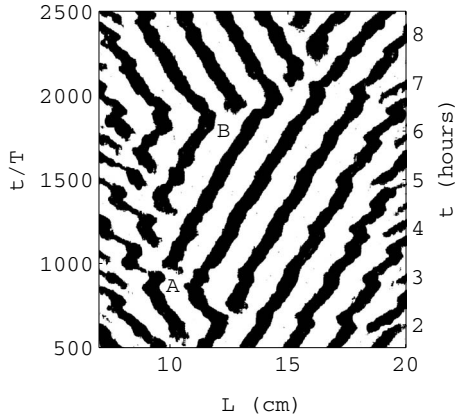

FIG. 6. Magnification of the section 7 cm$\leq L\leq$20 cm and $500\leq t/T\leq 2500$ of Fig. 5 for the spatiotemporal band-drift diagram of experiment GC8 ($\phi=16\%$).

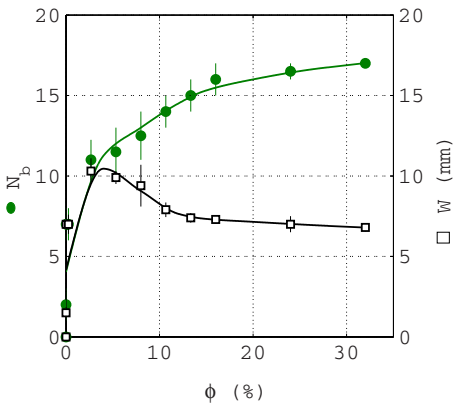

FIG. 8. (Color online) Number of bands, N_b, and band width, W, as a function of the concentration of particles ϕ.

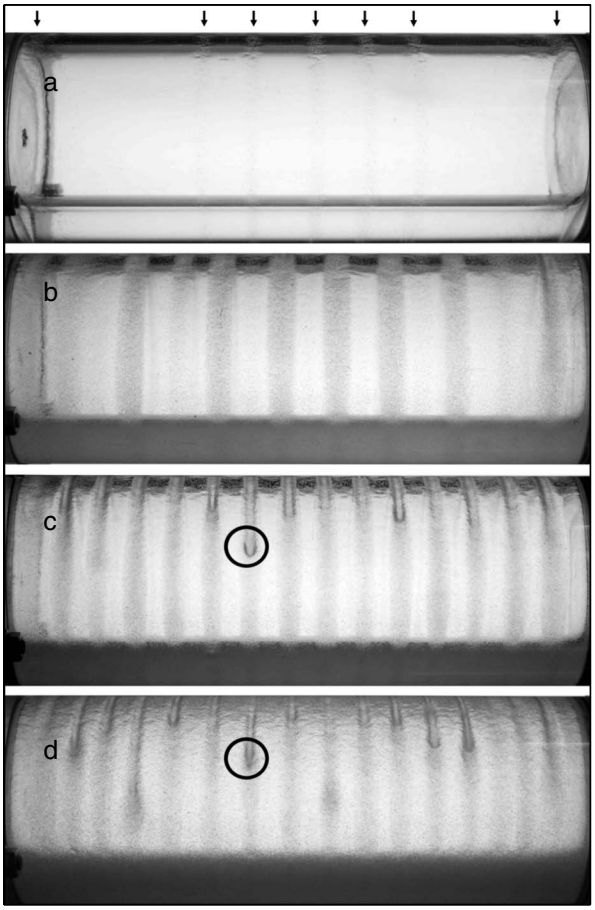

FIG. 9. Photographs of bands inside the cylinder for different granule concentrations. From top to bottom: ϕ=0.27% (GC3), 5.4% (GC5), 13.3% (GC7), and 32% (GC10). The black circles in (c) and (d) identify examples of forming droplets. The black arrows above (a) identify the positions of the very faint bands in experiment GC3.

2. Small wavelength changes induced by this concentration increase were negligible in comparison to the changes associated with the investigated increase of the rotation rate of the cylinder. Figure 8 also reveals that the band width, W, initially increases steeply with the particle concentration. The bandwidth adopts a maximum of approximately W =10 mm around ϕ=2.7%. It then decreases to just over W =6 mm at approximately ϕ=13%, whereupon it remains almost constant up to the highest concentration of ϕ=32%. Note from Fig. 8 that bands are widest for particle concentrations roughly equal to those that induce maximum band-drift velocities in Fig. 7.

A further feature associated with the increase of the particle concentration that has hitherto not been discussed in the literature is the formation of small droplets on the granule bands. Two examples of such droplets are identified in Figs. 9(c) and 9(d) where they are marked by black circles; several more droplets can be seen on other bands in these two photographs. The droplets form on the rising front of the rotating cylinder (facing the camera) and near its top. Once formed the drops begin to propagate downward along the bands on the rising cylinder front. It was observed that the rate at which droplets form depends on the particle concentration.

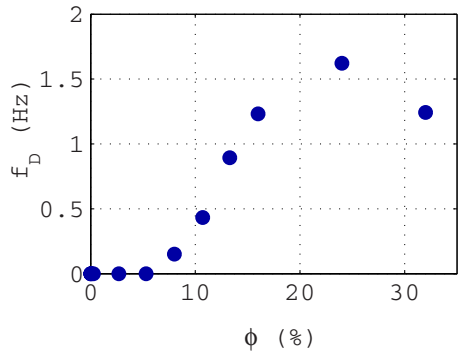

FIG. 10. (Color online) Mean droplet-formation frequency, f_D, as a function of the particle concentration, ϕ.

The mean droplet-formation frequency, f_D, is displayed in Fig. 10 as a function of ϕ. The figure reveals that droplets were first observed at ϕ=8% (RE). Note that this is close to the concentration value that yields maximum band-drift velocities in Fig. 7. In Fig. 10 the droplet-generation frequency initially increases with the particle concentration, it adopts a maximum around $\phi \approx 24\%$ and then decreases again. It is likely that the droplet formation in this series of experiments arises as a consequence of the action of gravitational forces associated with the increased effective density within the particle-rich regions on the granule bands.

C. Effects of the density and the size of the granules on the band-drift dynamics

1. Parameter regime of the experiments

To study the effects of changing the Stokes number, St, and the parameter δ on the band-drift dynamics a series of experiments with particles of different densities, ρ_g, and different diameters, d_g, were conducted.

The series referred to by GD (Granule Density) corresponds to experiments in which the mean particle diameter (d_g=338 μm) remained unchanged from RE while the particle density differs from that in RE. The materials used for GD are polyamide, sugar, and metal particles. The mass of granules added was selected to yield a value for the bulk granule concentration (ϕ=8%) equal to that of RE. Table IV summarizes the modified parameters for series GD. Photographs with typical flow patterns from series GD are shown in Figs. 11(a)–11(d).

TABLE IV. The density of the particles and the modified parameters for series GD.

	Expt.			
	GD1	GD2	RE	GD3
Materials	Polyamide 6	Sugar	Glass	Metal
ρ_g (g cm^{-3})	1.13	1.64	2.5	7.1
m (g)	27.1	39.4	60	170.4
St	0.0001	0.0026	0.0069	0.0297
f_D (Hz)	0	0	0.15	5

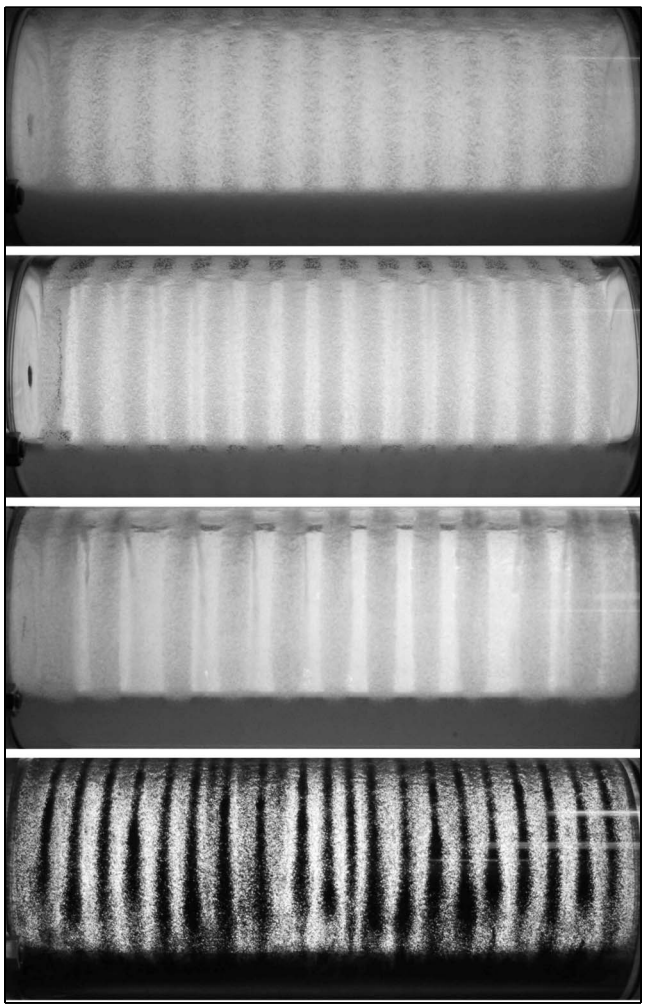

FIG. 11. Photographs of bands for particles with different densities, i.e., different Stokes numbers. From top to bottom: St=0.0001 (GD1), St =0.0026 (GD2), St=0.0069 (RE), St=0.0297 (GD3).

For another series of experiments, GDS (Granule Density Size), both the particle density and the particle size were changed simultaneously to further explore the parameter space in the δ and St domain. Note that increasing particle diameter implies an increasing settling velocity such that the Stokes number increases accordingly. The characteristic dimensions of the particles used in series GDS and the associated nondimensional numbers are summarized in Table V. Photographs with typical flow patterns from series GDS are shown in Figs. 12(a)–12(d).

2. Quantifying the ability of the bands to drift

Figure 13 shows a map for the experiments of series GD and GDS identifying whether or not band drift was observed. For all these experiments the axial segregation is not complete, there always remained some granules in the spaces between the bands. For the four experiments of series GD—which includes RE—band drift was observed in RE and GD3 where St $\geq$ 0.0069. The drift dynamics follow the same overall qualitative behavior patterns identified in connection with the other nondimensional parameters discussed in Sec. III B. However, for the other two experiments of the series, for

TABLE V. The sizes of the particles used in series GDS and the associated values of the affected nondimensional parameters.

Expt.	ρ_g (g cm^{-3})	$d_{\min}$ (μm)	$d_{\max}$ (μm)	δ	St	f_D (Hz)
GDS1	2.5	75	150	5.65	0.0008	0
GDS2	2.5	150	250	3.18	0.0024	0
GDS3	2.5	425	590	1.25	0.0154	1.4
GDS4	2.5	600	800	0.91	0.0296	2.5
GDS5	2.5	800	1000	0.71	0.0490	3.1
GDS6	2.5	1000	1200	0.58	0.0726	···
GDS7	1.6	400	600	1.27	0.0058	0
GDS8	1.6	600	800	0.91	0.0113	0.1
GDS9	1.6	800	1000	0.71	0.0188	0.8
GDS10	1.6	1250	1400	0.48	0.0407	1.5
GDS11	7.1	160	315	2.70	0.0147	3.4
GDS12	7.1	400	550	1.35	0.0587	8.1
GDS13	7.1	600	750	0.95	0.1184	···

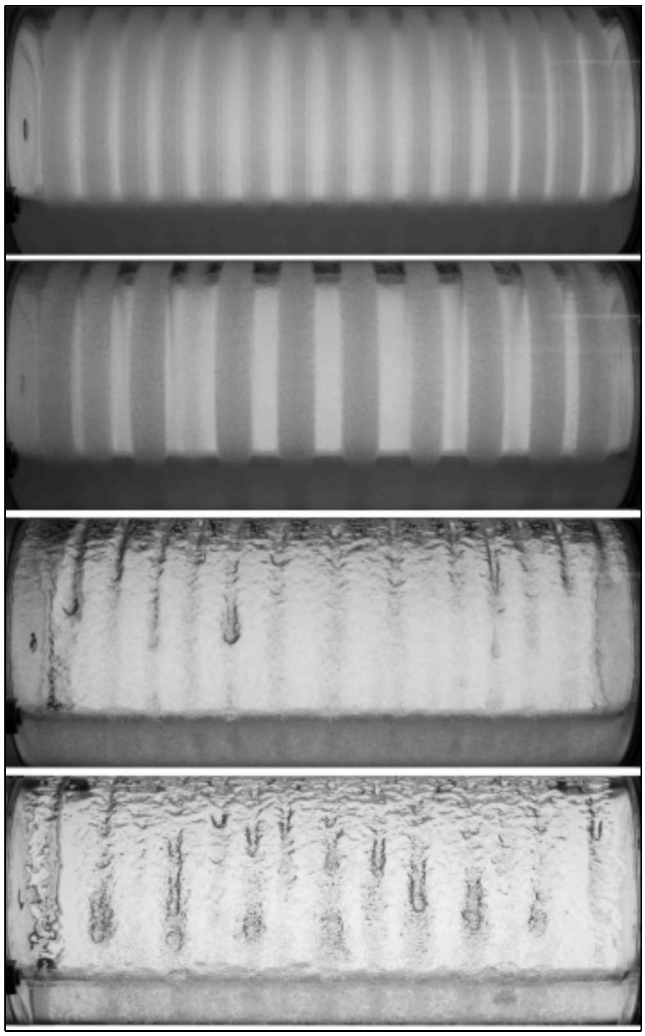

FIG. 12. Photographs of bands for particles with different diameters. From top to bottom: GDS1, GDS2, GDS4, and GDS6.

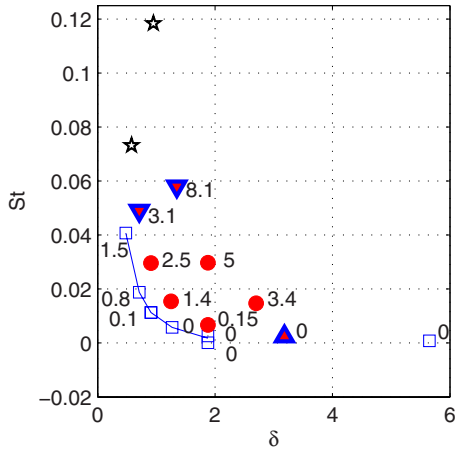

FIG. 13. (Color online) Diagram illustrating the drift mode of the bands in the St-δ domain: (●) Drifting always observed, (▲) unstable state where bands can be stationary, drifting or both, (□) bands always stationary, (▼) stationary central bands and drifting edge bands, (☆) bands do not form. The figures next to the markers identify the mean droplet-formation frequency, f_D, in units of hertz (●, bands always move; □, bands always stationary; ▲-▼, mixed states possible.)

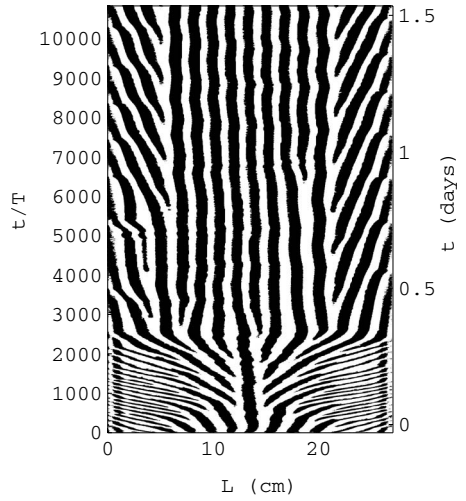

FIG. 14. Spatiotemporal evolution of the position of the granule bands in GDS2 with St=0.0024 and δ=3.18.

GD1 and GD2, where St$\leq$0.0026, the band-drift ceases. For the experimental conditions of GD1 and GD2 the bands were always stationary. This was verified by conducting several different runs under these experimental conditions with each run extending over several days. Hence, the results indicate that the critical Stokes number value above which band drift is initiated in the present experiment lies in the region between, roughly, St=0.0026 and St=0.0069.

Timberlake and Morris[6] reported fluctuating band motion for neutrally buoyant particles segregating in a horizontal Taylor–Couette system. This result appears to conflict with bands being stationary in GD1, where almost neutrally buoyant polyamide particles were used. However, the issue can be resolved by considering the differences between the present experimental setup and that in Ref. 6. In the Taylor–Couette system of[6] the overall main flow structure of the liquid must differ substantially from that developing in our cylinder. In the Taylor–Couette system the bounding end caps of the apparatus are fixed while only the inner cylinder rotates. However, the discussion in Sec. III B already revealed that the rotating end walls in our experimental setup almost certainly result in profound effects on the flow structure inside our cylinder and on the associated band-drift dynamics. This implies that a comparison of the flow in the Taylor–Couette system of Timberlake and Morris[6] with that in our rotating cylinder is not straightforward.

The data of the other series, GDS, enable further insight into the band-drift phenomenon. For GDS1, the experiment with the smallest particles and the lowest Stokes number (St=0.0001) the bands were found to be stationary. This is consistent with the stationary bands in experiment GD1 and GD2, where St$\leq$0.0026. In GD1 and GD2 the Stokes number was modified by means of the granule density alone whereas here in GDS1 it was altered through both size and density changes. This provides further support to the conclusion that the Stokes number is indeed a governing parameter as regards the initiation of band drift.

For the experimental conditions of GDS2 (second smallest particle class, St=0.0024, δ=3.18) it was discovered, through repeated runs under these conditions, that the space-time plots can display three different dynamic modes. For the conditions of GDS2 it was observed that sometimes all bands remained stationary, at other times the central bands were stationary while the bands closer to the end walls drifted and sometimes it was observed that all bands drifted. It was further found that transitions between the dynamic modes can occur during a single run as is illustrated in Fig. 14. In this particular case the figure shows that for times $t/T<2500$ all bands drifted outwards, i.e., toward the end walls. For $t/T>2500$ the system then adopted a state where only bands at $L<5$ cm and $L>21.4$ cm drifted outward while the central bands with 5 cm$\leq L\leq$21.4 cm remained stationary. In the sense of mode transitions becoming possible the experimental conditions of GDS2 can, thus, be regarded as unstable. Note that the value of the Stokes number of GDS2, which can display alternative drift modes, is of the same order of magnitude as the critical value (St=0.0026–0.0069) that separates the parameter regions of stationary and drifting bands in series GD.

A comparison of GDS2 with GD2 reveals the significance of the parameter $\delta=h_m/d_g$ which characterizes the ratio of the minimum thickness of the liquid film coating the inner cylinder wall and the particle diameter. GD2 (St=0.0026) and GDS2 (St=0.0024) have very similar values of the Stokes number, yet, under the conditions of GD2 the bands always remained stationary while band drift was possible in GDS2. The main difference between both experiments lies in the values of δ which were δ=3.18 for GDS2 and δ=1.88 for GD2. Hence, here a change in δ alone was sufficient to induce band drift. The particles in GD2 resulted in substantially larger surface deformations of the liquid film that coats the inside of the cylinder than the particles in GDS2. Larger surface deformations cause stronger surface-tension induced forces. It is reasonable to conclude that these forces result in a *stiffening* of the system and that they will consequently act toward reducing band drift.

As an aside, note that experiments GDS1 and GDS2, with the smallest particles, are the only two experiments of the present study which displayed thin side bands similar to those referred to as the fine structure by Thomas *et al.*[2] The side bands can be identified very faintly in Fig. 12(a) but they were not as well developed as those described by Thomas *et al.*[2]

Well-established band drift was also observed for GDS3 (St=0.0154, δ=1.25), for GDS4 (St=0.0296, δ=0.91), and for GDS11 (St=0.0147, δ=2.7). The overall spatiotemporal dynamics for all these experiments were very similar to those of RE shown in Fig. 2. Most importantly, however, we repeatedly observed that a change in δ alone was sufficient to suppress the band drift. Consider, for instance, the case of RE (St=0.007, δ=1.88), GDS8 (St=0.0113, δ=0.91) and GDS3 (St=0.0154, δ=1.25), for which St(RE)$<$St(GDS8)$<$St(GDS3). Here bands were always stationary for experiments with the intermediate Stokes number value of GDS8 whereas they always drifted for experiments with lower (RE) as well as higher (GDS3) Stokes number. For these three experiments δ(GDS8)$<\delta$(GDS3)$<\delta$(RE) and, thus, bands were stationary for the lowest δ of GDS8 but bands drifted for both of the two higher δ values of GDS3 and RE. Assuming that the system dynamics display a continuous and consistent response to variations of St and δ this suggests that, for these three experiments, it is not the Stokes number that governed the onset of band drift but, rather, the value of δ. An equivalent behavior in support of this is also displayed by, for instance, GDS3 (St=0.0154, δ=1.25, drifting), GDS9 (St=0.0188, δ=0.71, stationary), and GDS4 (St=0.0296, δ=0.91, drifting) where St(GDS3)$<$St(GDS9)$<$St(GDS4) and δ(GDS9)$<\delta$(GDS4)$<\delta$(GDS3).

For larger Stokes numbers, e.g., for GDS5 (St=0.049, δ=0.79) and GDS12 (St=0.0587, δ=1.35), the drift mode that is also seen for GDS2, which displays stationary central bands and drifting edge bands, is adopted. Here, however, we never observed the occurrence of drifting central bands or stationary edge bands. The Stokes number for these runs is, furthermore, large enough to induce strong circumferential asymmetries of the width of the bands. On the rising front of the cylinder the bands are now very wide compared to their width at the top of the cylinder. Accordingly the band thickness has to be larger on the rising front. This results in a reduced effective value for δ on the rising front of the cylinder and this may explain the stationary central bands.

Finally experiments GDS6 [Fig. 12(d)] and GDS13 may indicate a critical upper limit of the Stokes number for the occurrence of the segregation phenomena as such. For these two experiments, with St$>$0.07, the entire surface in the upper half of the cylinder was homogeneously covered with particles; this made it difficult to identify distinct bands there. However, as can be seen in Fig. 12(d), further downwards on the rising cylinder front band-type structures are more pronounced again. Here these become apparent through the type of droplets propagating downwards on the rising cylinder front similar to those in Figs. 9(c) and 9(d).

In summary, then, the ability of the bands to drift depends on both the Stokes number, St, and the parameter δ. The bands become stationary whenever either one of these two parameters becomes too small. The dependence of the band drift on δ suggests the existence of strong surface-tension effects. As δ becomes small the particle interaction with the free surface of the liquid film becomes important. The results obtained thus suggest that the capillary forces induced by the film deformation may be so strong that particle motions are inhibited and, as a consequence, the forces act to suppress the band drift.

3. Droplet formation

Similar to series GC in Sec. III B we observed droplet formation in series GD and GDS. The formation frequency was measured for each experiment and the results obtained are included in Fig. 13 where the mean droplet-formation frequencies, f_D, are identified by the numbers next to each of the markers. The number of droplets forming increases with increasing Stokes number; as one would anticipate. No drops were observed in GD2 whereas the formation frequency reached up to 5 Hz in GD3. Moreover for a fixed value of the Stokes number, the parameter δ also affects the droplet formation. Small, dense particles result in the formation of more droplets per unit time than large, light particles. As regards this compare, for instance, GDS4 ($600\ \mu\text{m} \leq d_g \leq 800\ \mu\text{m}, \rho_g=2.5\ \text{g cm}^{-3}$), where $f_D=2.5$ Hz and GD3 (mean $d_g=338\ \mu$m, $\rho_g=2.5\ \text{g cm}^{-3}$), where $f_D=5$ Hz.

IV. CONCLUSION

Eight nondimensional parameters are required to characterize the drift dynamics of segregation bands forming in particle-laden rimming flow. We first documented, and qualitatively discussed, the often very complex and highly symmetric spatiotemporal drift dynamics by Guyez and Thomas.[11] Here we began to experimentally study the effects of the variation of three of the governing nondimensional parameters in detail. We have investigated effects of the bulk concentration of the suspended particles (ϕ), effects of the ratio of the minimum thickness of the liquid film covering the inside of the cylinder and the particle diameter (δ), as well as effects of the Stokes number (St).

It was found that whether bands can or cannot drift depends on both the Stokes number and the parameter δ. The bands were observed to become stationary whenever one of these two parameters becomes too small. The dependence of the band drift on δ does in particular suggest the existence of strong surface-tension effects. As δ becomes small the particle interaction with the free surface of the liquid film becomes more pronounced. It was argued that the capillary forces induced by the film deformation tend to act toward inhibiting particle motions and, hence, band drift.

Within the parameter regime of St and δ where band drift is possible the band-drift velocity depends on ϕ. It was found that the band-drift velocity adopts a maximum near the end walls which was, in the case of the liquid and particles used here, reached around $\phi \approx 5\%$. It was argued that the existence of a maximum drift velocity is probably the consequence of two competing effects. For lower particle concentrations a rising concentration probably leads to stronger particle-particle and band interactions resulting in higher

drift velocities. However, increasing particle concentrations also result in a higher effective viscosity of the particle-laden liquid. It appears plausible that above the value of ϕ which yields the highest drift velocity the decelerating effects of a viscosity increase outweigh the accelerating particle and band-interaction effects resulting in an overall net reduction of the drift speeds. For the value of ϕ that yielded maximum drift velocities it was further observed that the width of the bands also adopts maximum values. For increasing concentrations the band width decreases and the overall band-drift dynamics become more synchronized.

We emphasize in particular that the drift direction of the bands is not sensitive to the variations of the particle concentration, the particle size, and the particle density studied here. In all present experiments the band drift was directed from the central portion of the cylinder toward the end walls. New bands were not observed to form adjacent to the end walls. None of the present experiments displayed the mode documented by Guyez and Thomas,[11] where bands drift from the end walls toward the cylinder center and where the situation is reversed and new bands typically form close to the end walls. Together with the observed accelerated band drift in the proximity of the end walls this suggests that the flow dynamics near the end walls and, consequently, the aspect ratio of the cylinder play key roles in establishing and sustaining the drift of the segregation bands. The near-wall flow dynamics will be affected by the fluid properties and these may therefore also affect the selection of the drift mode.

Finally we briefly discussed a feature of the flow that has not been addressed in any previous publication on the subject. We observed the formation of small droplets near the top of the cylinder under certain experimental conditions. Droplets were found to form for large Stokes numbers, large values of δ as well as for large granule concentrations, ϕ. It was discussed that for large Stokes numbers the droplets form as a result of their large weight and, thus, from large gravitational forces acting upon the individual granules. In the remaining cases it appears that the drops form as a result of increased net densities and, thus, strong gravitational forces in regions of high particle concentrations.

Unfortunately we do not yet have results available for experiments with negative Stokes numbers, i.e., for particles that are less dense than the ambient liquid. The absence of these results is due to us not being able to locate a supplier of light particles with appropriate, i.e., sufficiently large, mean diameters. The small, light particles available in our laboratory, used by Thomas *et al.*,[2] have diameters that yield Stokes numbers close to zero under conditions where the other nondimensional parameters would remain unaltered.

[1] O. A. M. Boote and P. J. Thomas "Effects of granular additives on transition boundaries between flow states of rimming flows," Phys. Fluids **11**,2020 (1999).
[2] P. J. Thomas, G. D. Riddell, S. Kooner, and G. P. King, "Fine structure of granular banding in two-phase rimming flow," Phys. Fluids **13**, 2720 (2001).
[3] J. Lee and A. J. C. Ladd, "Axial segregation of a settling suspensions in a rotating cylinder," Phys. Rev. Lett. **95**, 048001 (2005).
[4] G. Seiden, M. Ungarish, and S. G. Lipson, "Banding of suspended particles in a rotating fluid-filled horizontal cylinder," Phys. Rev. E **72**, 021407 (2005).
[5] M. Tirumkudulu, A. Tripathi, and A. Acrivos, "Particle segregation in monodisperse sheared suspensions," Phys. Fluids **11**, 507 (1999).
[6] B. D. Timberlake and J. F. Morris, "Concentration band dynamics in free-surface Couette flow of a suspension," Phys. Fluids **14**, 1580 (2002).
[7] B. D. Timberlake and J. F. Morris, "Film depth and concentration banding in free-surface Couette flow of a suspension," Philos. Trans. R. Soc. London, Ser. A **361**, 895 (2003).
[8] M. Tirumkudulu, A. Mileo, and A. Acrivos, "Particle segregation in monodisperse sheared suspensions in a partially filled rotating horizontal cylinder," Phys. Fluids **12**, 1615 (2000).
[9] B. Jin and A. Acrivos, "Rimming flows with an axially varying viscosity," Phys. Fluids **16**, 633 (2004).
[10] B. Jin and A. Acrivos, "Theory of particle segregation in rimming flows of suspensions containing neutrally buoyant particles," Phys. Fluids **16**, 641 (2004).
[11] E. Guyez and P. J. Thomas, "Spatiotemporal segregation-pattern drift in particle-laden rimming flow," Phys. Rev. Lett. **100**, 074501 (2008).
[12] D. D. Joseph, J. Wang, R. Bai, B. H. Yang, and H. H. Hu, "Particle motion in a liquid film rimming the inside of a partially filled rotating cylinder," J. Fluid Mech. **496**, 139 (2003).